Cyclotron-Bloch dynamics of a quantum particle in a two-dimensional lattice. II. Arbitrary electric field directions

Andrey R. Kolovsky,[1,2] Ilya Chesnokov,[2] and Giorgio Mantica[3,4,5]
[1]*Kirensky Institute of Physics, 660036 Krasnoyarsk, Russia*
[2]*Siberian Federal University, 660041 Krasnoyarsk, Russia*
[3]*Center for Nonlinear and Complex Systems, Department of Science and High Technology, University of Insubria, 22100 Como, Italy*
[4]*I.N.F.N. sezione di Milano, Italy*
[5]*CNISM unità di Como, Italy*
(Received 25 May 2012; published 25 October 2012)

We study the quantum dynamics of a charged particle in a two-dimensional lattice, subject to constant and homogeneous electric and magnetic fields. We find that different regimes characterize these motions, depending on a combination of conditions, corresponding to weak and strong electric field intensities, rational or irrational directions of the electric field with respect to the lattice, and small or large values of the magnetic (Peierls) phase.

DOI: 10.1103/PhysRevE.86.041146 PACS number(s): 05.60.Gg, 72.10.Bg, 73.43.−f

I. INTRODUCTION AND STATEMENT OF RESULTS

This is the second paper in a row on the quantum dynamics of a charged particle in a two-dimensional square lattice, under the influence of an in-plane electric field and a normal to the plane magnetic field, both uniform in space and constant in time. In a previous work [1] we considered the case where the electric field is aligned with one of the lattice axes. We now extend this investigation to arbitrary directions of the electric field, still lying on the lattice plane. New phenomena are found in this generalization.

Many physical systems, including Bose condensates in optical lattices, can be described by the Hamiltonian $\widehat{H}$ of a charged particle in a two-dimensional lattice oriented as the reference frame (x,y), in the tight-binding approximation [1]:

$$(\widehat{H}\psi)_{l,m} = -\frac{J_x}{2}(e^{-i2\pi\alpha m}\psi_{l+1,m} + e^{i2\pi\alpha m}\psi_{l-1,m}) - \frac{J_y}{2}(\psi_{l,m+1} + \psi_{l,m-1}) + ea(F_x l + F_y m)\psi_{m,l}, \tag{1}$$

which is written here for the Landau gauge $\mathbf{A} = B(-y,0)$. In the above, ψ is the wave function, the integer pair (l,m) labels the lattice site $(x,y) = (la,ma)$ in which a is the lattice period, J_x, J_y are the hopping matrix elements, F_x, F_y are the electric field components, B is the intensity of the magnetic field, e is the charge, and α is the *Peierls phase*, defined as the ratio between the magnetic flux through the unit cell, Ba^2, and the elementary flux hc/e. A second ratio is crucial in this Hamiltonian, that between the Bloch frequencies $\omega_x = eaF_x/\hbar$ and $\omega_y = eaF_y/\hbar$ associated with the two components of the electric field vector. For convenience we call $\beta = \omega_x/\omega_y$ the *(electric) field orientation*. These two ratios deserve to be clearly marked for further use:

$$\alpha := eBa^2/hc, \quad \beta := \omega_x/\omega_y = F_x/F_y. \tag{2}$$

The content of this paper is a detailed study of the dynamics generated by the above Hamiltonian. These dynamics are far from trivial even when one of the fields is absent. In fact, for vanishing magnetic field the wave-packet motion features Bloch oscillations, which crucially depend on the rationality of the electric field orientation β. In the opposite case of null electric field, a commensurability condition still appears, this time in terms of the Peierls phase α. Clearly, the problem becomes even subtler when both fields are present. To some extent, this problem has been considered earlier. We would like to mention Ref. [2], a seminal paper that introduced the method of rotated coordinate frame discussed below; Ref. [3], which studied conductivity in a lattice with anisotropic hopping; Ref. [4], where delocalization in the direction orthogonal to the electric field, for certain rational field orientations and intensities, was described; Ref. [5], where the physical case of a two-dimensional array of quantum dots in GaAs was considered; and finally, Ref. [6], in which numerical experiments on the motion of wave packets revealed interesting vortex-like behaviors.

Given these premises, our aim is to construct a complete theory of all dynamical regimes present in this system. In the previous paper [1] we have analyzed the semiclassical region $|\alpha| \ll 1$, for the particular case when the electric field is aligned with one of crystallographic axes of a square lattice; that is, we examined the case $\beta = 0$. In this work we extend these studies to arbitrary directions of the electric field vector and to arbitrary magnetic field intensities. This yields a three-parameter space (F,α,β) (F is the amplitude of the electric field) characterized by various dynamical behaviors. We elect not to vary a further parameter, the ratio between couplings in the two orthogonal directions of the lattice, J_x and J_y, keeping them equal to J [7]. Also, without any loss of generality, we assume $|\alpha| \leqslant 1/2$ and $0 \leqslant \beta \leqslant 1$.

Our results can be summarized as follows. In Sec. III we first focus on the case of small α, where we can use a semiclassical approach in which the Peierls phase α plays the role of an effective Planck constant. We derive the one-dimensional classical Hamiltonian

$$H_{\rm cl} = -J_y\cos P - J_x\cos Y + \mathcal{F}_x P + \mathcal{F}_y Y, \qquad \mathcal{F}_{x,y} = \frac{eaF_{x,y}}{2\pi\alpha}, \tag{3}$$

as an approximation of the Hamiltonian (1). We find that both classical and quantum dynamics strongly depend on whether

the following conditions hold:

$$\mathcal{F}_x < J_x \quad \text{and} \quad \mathcal{F}_y < J_y. \tag{4}$$

First of all, when the above are verified, a stable island gives rise to classical streaming across the lattice, in the direction orthogonal to the electric field, with velocity v^* given by

$$v^* = ea^2 F/h\alpha. \tag{5}$$

Since semiclassical theory is applicable whenever the Peierls phase α is much smaller than one, we therefore predict that when

$$eaF/2\pi J < \alpha \ll 1 \tag{6}$$

the quantum motion generated by the Hamiltonian (1) allows for wave packets traveling at speed v^* for any value of the direction ratio β, at least for a finite time span that increases as α tends to zero. Conditions (6) therefore define the *small-field, semiclassical regime*.

We then turn to a purely quantum analysis. In Sec. IV we start by examining the case of rational orientation β and we argue that for nonzero electric field the spectrum of (1) is absolutely continuous for any value of α. We describe two techniques to compute this spectrum, which can also be implemented numerically. Next, using spectral analysis, when (6) holds, we construct the Stark transporting states (already defined for $\beta = 0$ in [1]), which quantize the semiclassical transporting islands of Hamiltonian (3). We show that their evolution is characterized by linear motion with speed v^*. Also in Sec. IV, we use perturbation theory to compute, to leading order in the inverse field amplitude $1/F$, the width of the energy bands of the Hamiltonian (1). Letting $\beta = r/q$, with r,q co-prime integers, we find that these widths scale as $(1/F)^{q+r-1}$. This suggests that the energy spectrum of this Hamiltonian is *pure point* for irrational direction ratio β. Note that being based on quantum perturbation theory, these results are not restricted to the semiclassical region.

We then turn to the numerical simulation of the time evolution of an initial wave packet, to confirm the theoretical predictions of the spectral analysis. The numerical techniques are briefly described in Sec. V. They permit us to attack the most general case, which includes nonrational directions of the electric field. First, we consider the case $F \gg F_{\rm cr} \equiv 2\pi\alpha J/ea$, where we can apply the perturbation theory of Sec. IV, and show that an initial wave packet spreads in the direction orthogonal to the electric field with a dispersion σ that increases in time as

$$\sigma \sim (1/F)^{(q+r-1)}t \tag{7}$$

(here, as above, $\beta = r/q$). This behavior sets in after a transient time

$$\tau \sim F^{(q+r-1)}, \tag{8}$$

during which the packet is localized. Thus for irrational field directions the wave packet is always localized in the lattice, which is consistent with discreteness of the spectrum for irrational β.

Next, in Sec. VI we describe the case $F < F_{\rm cr}$ for the semiclassical region $|\alpha| \ll 1$. We find that the motion is either a ballistic spreading (for an incoherent initial wave packet) or directed transport (for a properly devised coherent initial wave packet), both for rational and irrational directions β, for all times that we could reach in our numerical simulations. This seems to be inconsistent with discreteness of the spectrum for irrational β. To resolve this seemingly contradiction we turn in Sec. VII to the case of arbitrary values of the Peierls phase α. We simulate the quantum evolution for an increasing sequence of values of α while keeping the classical parameters $\mathcal{F}_x$ and $\mathcal{F}_y$ fixed. For irrational directions β, at fixed time, we observe a sharp suppression of ballistic spreading, occurring when α overcomes a certain threshold. Turning finally to a time-resolved analysis, we observe saturation of the ballistic spreading, for times larger than a threshold that grows abruptly with the inverse of the electric field intensity F. Combined with the observation on bandwidths, this fact strengthens the conjecture that the spectrum of the system is pure point, for any irrational direction β—yet the localization length should depend sensitively on the magnitude of the electric field F, like in certain two-dimensional models of quantum rotators and of Anderson localization [8–10]. This concludes our analysis of this system.

II. ALIGNED ELECTRIC FIELD: REVIEW OF RESULTS

To introduce concepts and notations, we now briefly review the results of our previous work [1], where we considered the case of an electric field $\mathbf{F} = (0, F)$ aligned with the y axis of a reference frame defined by a two-dimensional square lattice. The magnetic field is directed orthogonally to the lattice plane, and the Peierls phase α is small. The system shows two qualitatively different dynamical regimes, depending on the magnitude of the electric field: a regime of directed transport for weak fields and a regime of ballistic spreading for strong fields, separated by a critical magnitude, $F_{\rm cr} = 2\pi\alpha J_x/ea$. Although we will keep track of physical constants for completeness in what follows, in numerical experiments we adopt adimensional units so that $e = a = \hbar = 1$ and we set $J_x = J_y = 1$. Also, until Sec. VII or unless otherwise noted, the Peierls phase is $\alpha = 1/10$.

A. The energy spectrum

The stationary Schrödinger equation derived from Eq. (1) is

$$-\frac{J_x}{2}(e^{-i2\pi\alpha m}\psi_{l+1,m} + e^{i2\pi\alpha m}\psi_{l-1,m}) - \frac{J_y}{2}(\psi_{l,m+1} + \psi_{l,m-1}) + eaFm\psi_{l,m} = E\psi_{l,m}. \tag{9}$$

Imposing a periodicity of period $L_x = La$ in the l direction in Eq. (9), where L eventually tends to infinity, and using the substitution $\psi_{l,m} = \frac{e^{i\kappa al}}{\sqrt{L}} b_m(\kappa)$, where κ is the dimensional quasimomentum, $\kappa = 2\pi k/aL$, with $k = 0, 1, \ldots, L-1$, taking values in $[0, 2\pi/a)$, one reduces (9) to the following 1D equation for the coefficients $b_m(\kappa)$:

$$-\frac{J_y}{2}(b_{m+1} + b_{m-1}) - J_x \cos(2\pi\alpha m - a\kappa)b_m + eaFmb_m = Eb_m. \tag{10}$$

The spectrum of (10) for a fixed κ is a modulated Wannier-Stark ladder and the energy bands appear by varying the quasimomentum. For example and for the purpose of future

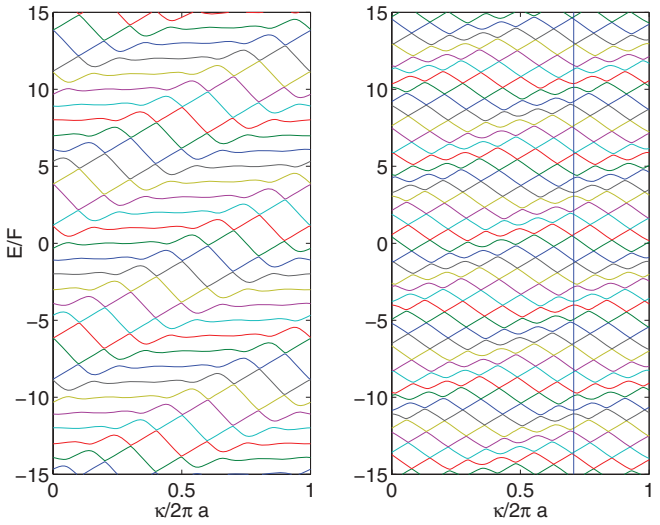

FIG. 1. (Color online) The energy spectrum $E = E_\nu(\kappa)$ for $F = 0.3$ and $(r,q) = (0,1)$ (left) and $(r,q) = (1,1)$ (right). The vertical line in the right panel marks the first Brillouin zone, the size of which scales as $1/\sqrt{r^2+q^2}$. Different colors have no particular meaning but are used to better distinguish the lines, which are nonintersecting.

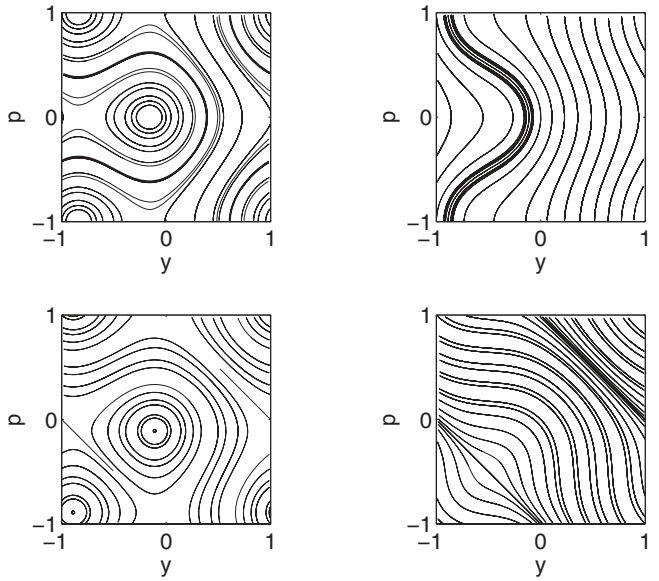

FIG. 2. Phase portrait of the classical system (14) for $(r,q) = (0,1)$ (upper row) and $(r,q) = (1,1)$ (lower row) at electric field intensities $F = 0.3$ (left column) and $F = 1$ (right column). Twenty different trajectories are shown in each case.

comparison, the left panel of Fig. 1 shows the eigenvalues $E_\nu(\kappa)$ of this equation for $F = 0.3$. To understand the displayed spectrum the semiclassical approach proves to be very useful.

B. Semiclassical theory

When $|\alpha|$ is much less than one, the period of the oscillating phase in Eq. (10) is much larger than the lattice period, so that we can approximate the discrete function b_m by a continuous function $\mathcal{B}$ of the coordinate y. Furthermore, consider the shift operator $\widehat{T}_a = \exp(a\partial_y)$, which acts as $\widehat{T}_a\mathcal{B}(y) = \mathcal{B}(y+a)$. Using this in Eq. (10) leads to

$$[-J_y\cos(ia\partial_y) - J_x\cos(2\pi\alpha y/a - a\kappa) + eFy]\mathcal{B}(y) = E\mathcal{B}(y).$$

Next, introducing the operators $\widehat{Y} = 2\pi\alpha y/a$ and $\widehat{P} = -ia\partial_y$ in the above leads us to the effective Hamiltonian $\widehat{H}_{qu} = -J_y\cos\widehat{P} - J_x\cos(\widehat{Y} - a\kappa) + \mathcal{F}\widehat{Y}$, whose classical counterpart reads

$$H_{\rm cl} = -J_y\cos P - J_x\cos Y + \mathcal{F}Y, \quad \mathcal{F} = \frac{eaF}{2\pi\alpha}. \tag{11}$$

Since in the quantum description the canonical variables P,Y are operators obeying the commutation relation $[\hat{Y},\hat{P}] = i2\pi\alpha$, the semiclassical parameter is here the Peierls phase α. If $|\alpha| \ll 1$, one can explain certain features of the spectrum in Fig. 1(a) by simply analyzing the phase portraits of the classical system (11). In particular, it is easy to see that the Hamiltonian (11) can support bounded motions if $F < F_{\rm cr}$. These are seen as the islands around the fixed points in Fig. 2, upper row, which draw the solutions of Hamilton equations for the Hamiltonian $H_{\rm cl}$, Eq. (11).

By introducing the Bloch frequency $\omega = eaF/\hbar$ and using the canonical substitution $P \to P - \omega t$, one obtains from (11) the time-dependent Hamiltonian

$$H_{\rm cl}(t) = -J'_y\cos(P - \omega t) - J'_x\cos Y, \quad J_{x,y} = 2\pi\alpha J_{x,y}, \tag{12}$$

in which the canonical variables lie in the torus, $-\pi \leqslant P,Y < \pi$. The classical phase space of solutions of (11), pictured in Fig. 2, can also be calculated as the stroboscopic map of the time-periodic Hamiltonian (12). Two cases for $F < F_{\rm cr}$ and $F > F_{\rm cr}$ are shown in Fig. 2. Bounded trajectories of (11) appear now as two nonlinear resonances (transporting islands), whose size shrinks to zero when $F = F_{\rm cr}$. Quantizing these islands leads to the transporting modes, defined below.

Note that in Ref. [1] a different gauge, $\mathbf{A} = B(0,x)$, was employed. Needless to say, the quantum spectrum of the system does not depend on the gauge adopted. In classical mechanics, the latter gauge corresponds to the Hamiltonian $\bar{H}_{\rm cl}(t) = -J'_x\cos P - J'_y\cos(X + \omega t)$, that can be obtained from (12) by a canonical transformation that interchanges the role of P as momentum and Y as coordinate.

C. Directed transport regime

When F is small, the energy bands $E(\kappa)$ overlap forming a rather complicated band pattern. If $F < F_{\rm cr}$ this pattern contains a number of parallel straight lines, seen in Fig. 1(a). In the semiclassical approach these lines are associated with nonlinear resonances, which transport the particle at the drift velocity (5). The explicit form of the quantum transporting states is

$$\Psi_{l,m} = \int g(\kappa)e^{i\kappa al}b_m(\kappa)d\kappa, \tag{13}$$

where $\mathbf{b}(\kappa)$ is the eigenvector of (10) associated with a given straight line in the energy spectrum and $g(k)$ is an arbitrary square integrable function of the quasimomentum. Note that in $\mathbf{b}(\kappa)$ we jump over avoided crossings when following a straight

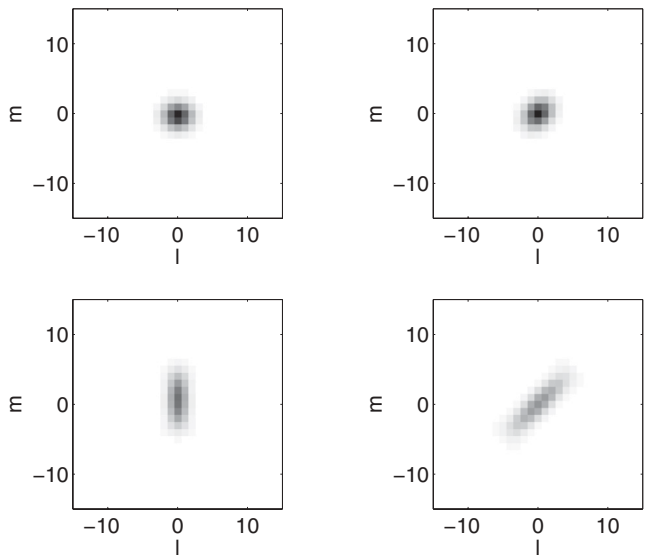

FIG. 3. Example of transporting states $|\Psi_{l,m}|^2$ for $(r,q) = (0,1)$ (left column) and $(r,q) = (1,1)$ (right column) depicted as grey tone images (black maximum, linear intensity scale). The upper row is characterized by the width parameter $C = 1$, while the lower row has $C = 0.2$. The other parameters are $\alpha = 0.1$ and $F = 0.1$.

line in $E(\kappa)$. This is the so-called diabatic approximation. Thus the vector function $\mathbf{b}(\kappa)$ in Eq. (13), which implicitly assumes the extended Brillouin zone picture, satisfies the translational relation

$$b_m(\kappa + 2\pi/a) \approx b_{m+1/\alpha}(\kappa),$$

which is exact if $1/\alpha$ is an integer. This relation should be compared with the relation $b_m(\kappa + 2\pi/a) = b_m(\kappa)$ which holds when we follow the energy bands adiabatically.

The left row in Fig. 3 shows numerically transporting states for $g(\kappa) \sim \exp[-C(a\kappa/2\pi)^2]$ for two different values of the parameter C [11]. Since the slope of the straight lines in the spectrum is equal to the drift velocity, the time evolution of these states is a shift of the wave packet in the x direction at velocity v^*. Thus the wave-packet width σ is constant in time, while the first moment grows as $M_1(t) = v^*t$. Here and below we identify the wave-packet width with the dispersion, i.e., $\sigma = \sqrt{M_2 - M_1^2}$, where $M_i, i = 1,2$, are the first two moments of the position operator.

It is worth stressing that the above statement refers only to initial conditions given in Eq. (13). For a generic initial wave packet one observes an asymmetric ballistic spreading (see Fig. 10 in Ref. [1]), where $M_1(t) \approx 0$ and $\sigma(t) \to At$. The coefficient A is here defined by the drift velocity, $A \sim v^* \sim F$, and *not* by the hopping matrix element J_x as in the strong-field regime described in the next subsection.

D. Ballistic spreading regime

Consider the strong-field limit, $eaF \gg J_{x,y}$. Using first-order perturbation theory the solution of (10) reads

$$E_\nu(\kappa) = eaF\nu - J_x \cos(a\kappa + 2\pi\alpha\nu),$$
$$b_m^{(\nu)}(\kappa) = \delta_{\nu,m} \pm (J_y/eaF)\delta_{\nu,m\pm1}.$$

It follows from the above equations that the time evolution of a generic localized wave packet is a ballistic spreading in the positive and negative x directions, so that the packet width σ grows asymptotically as $\sigma(t) = At$. The numerical factor A in this asymptotic expression depends on the particular form of the initial wave packet, yet it is superiorly bounded by $A = J_x/\sqrt{2}$. The maximal value is reached for an incoherent wave packet, which we can mimic by assigning random phases to the complex amplitudes of an initial Gaussian wave packet. Further down in this paper, Fig. 8 displays the F dependence of the coefficient A, obtained by direct numerical simulation of the system dynamics, versus $F = F_y$. The coefficient A tends to zero in the limit of weak electric fields, while in the opposite limit of strong fields it approaches the constant value $A = J_x/\sqrt{2}$. We will now investigate how this situation changes when the electric field is not aligned with one of the axes of the crystal.

III. GENERAL DIRECTION OF THE ELECTRIC FIELD: SEMICLASSICAL THEORY

The classical Hamiltonian (3) for generic direction of the electric field,

$$H_{\rm cl} = -J_y \cos P - J_x \cos Y + \mathcal{F}_y Y + \mathcal{F}_x P,$$
$$\mathcal{F}_{x,y} = \frac{eaF_{x,y}}{2\pi\alpha}, \tag{14}$$

can be guessed a straightforward generalization of the classical Hamiltonian (11). More rigorously, the same expression can be obtained as done in Appendix, starting from the quantum equation (21) below. Again, it is convenient to use the canonical transformation $P \to P - \omega_y t$ and $Y \to Y + \omega_x t$, which leads to the time-dependent Hamiltonian

$$H_{\rm cl}(t) = -J_y' \cos(P - \omega_y t) - J_x' \cos(Y + \omega_x t),$$
$$J_{x,y}' = 2\pi\alpha J_{x,y}. \tag{15}$$

Now the phase space of the system (15) can be reduced to the torus only when two Bloch frequencies ω_x and ω_y are commensurate, i.e., if $\beta := \omega_x/\omega_y = F_x/F_y = r/q$ (r,q are co-prime integers). However, semiclassical analysis can be applied equally well in the both cases of rational and irrational β. Let us also note that the system (15) has the global integral of the motion,

$$\mathcal{I} = H_{\rm cl}(t) + \mathcal{F}_y Y + \mathcal{F}_x P,$$

that reflects the fact that the original Hamiltonian Eq. (3) or Eq. (14) is one-dimensional and hence is trivially integrable, for any value of the ratio β.

The lower panels in Fig. 2 show the classical phase space for $\beta = 1$: Classical islands appear for small field magnitudes. The structure of phase space changes when the field magnitude is increased, similar to what happens in the case $\beta = 0$ (higher panels). The transporting islands disappear when at least one of the two conditions $\mathcal{F}_x < J_y$ and $\mathcal{F}_y < J_y$ is violated; this yields the condition (4). This result indicates that the original quantum system must have two qualitatively different regimes, which are separated by a critical field magnitude $F_{\rm cr} = 2\pi\alpha J/ea$. This conjecture is supported by analysis of

the energy spectrum of the quantum system, which we consider now, starting from the case of rational orientation β.

IV. ENERGY SPECTRUM FOR RATIONAL ORIENTATION OF THE ELECTRIC FIELD

We now proceed to the case of arbitrary, yet rational, direction of the vector $\mathbf{F} = (F_x, F_y)$. We first review two techniques to compute the energy spectrum in the case of rational ratio $\beta = F_x/F_y$. This analysis facilitates the understanding of the wave-packet dynamics, which will be described in Sec. V. Letting r and q be relatively prime integer numbers, we align the electric field with the (r,q) direction in the plane:

$$\mathbf{F} = \frac{F}{\sqrt{N}}(r,q), \tag{16}$$

where $N = r^2 + q^2$. We choose the gauge

$$\mathbf{A} = B\left(-\frac{q(rx+qy)}{r^2+q^2}, \frac{r(rx+qy)}{r^2+q^2}\right), \tag{17}$$

which reflects the geometry induced by the electric field. Within this gauge, the Hamiltonian becomes

$$\begin{aligned}(\widehat{H}\psi)_{l,m} = &-\frac{J_x}{2}\left(\exp\left[-i2\pi\alpha\frac{q}{N}(rl+qm)\right]\psi_{l+1,m} + \text{H.c.}\right)\\ &-\frac{J_y}{2}\left(\exp\left[i2\pi\alpha\frac{r}{N}(rl+qm)\right]\psi_{l,m+1} + \text{H.c.}\right)\\ &+eaF\frac{(rl+qm)}{\sqrt{N}}\psi_{l,m},\end{aligned} \tag{18}$$

where H.c. denotes the terms required to render the Hamiltonian Hermitian.

The calculation of the energy spectrum can be equally achieved by either of two different yet equivalent methods, which we shall refer to as the method of rotated coordinate frame, introduced in [2], and the method of rotated basis.

A. Rotated coordinate frame

The method of rotated coordinate frame [2] consists of two steps. The first is to choose the previous gauge, Eq. (17), for the magnetic field. The second step is to simplify the Hamiltonian (18) by rotating coordinates to align the electric field with the vertical axis ξ of a new coordinate frame (η,ξ):

$$\eta = \frac{qx - ry}{\sqrt{r^2+q^2}}, \quad \xi = \frac{rx+qy}{\sqrt{r^2+q^2}}. \tag{19}$$

In the rotated coordinates, the original lattice sites (al,am), with integer l and m, appear to lie on a sublattice immersed into a new square lattice of spacing d,

$$d = a/\sqrt{N},$$

whose sites (sd,pd) can be labeled by pair of integer indexes (s,p). Note that this new lattice actually consists of N independent sublattices, only one of which coincides with the original lattice; see Fig. 4. Explicitly, the mapping of the original lattice that points into the new, extended lattice is

$$(l,m) \to (ql - rm, rl + qm) := (s,p),$$

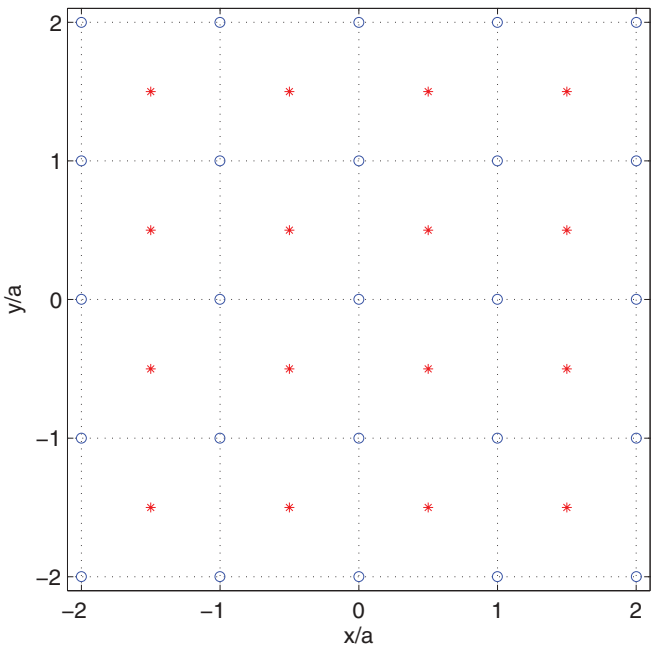

FIG. 4. (Color online) Extended lattice for the field direction $(r,q) = (1,1)$, where it consists of two sublattices (blue circles and red stars, respectively).

while the inverse mapping reads

$$(s,p) \to \frac{1}{N}(qp - rs, qs - rp) := (l,m).$$

Letting now $\phi_{s,p}$ denote the wave-function amplitude at site (sd,pd) in the rotated frame of reference (η,ξ), and using the fact that $(rl + qm) = p$, we can write the Hamiltonian action as

$$\begin{aligned}(\widehat{H}\phi)_{s,p} = &-\frac{J_x}{2}(e^{-i2\pi\alpha qp/N}\phi_{s+q,p+r} + \text{H.c.})\\ &-\frac{J_y}{2}(e^{i2\pi\alpha rp/N}\phi_{s-r,p+q} + \text{H.c.}) + edFp\phi_{s,p}.\end{aligned} \tag{20}$$

Observe that, coherently with Eq. (18), the N sublattices described above are uncoupled, and that the shift $s \to s + N$ is an invariant transformation. Nevertheless, it is convenient to solve the eigenvalue problem for all sublattices simultaneously. We therefore consider the stationary Schrödinger equation for the complex amplitudes ϕ, $(\widehat{H}\phi)_{s,p} = E\phi_{s,p}$. Following [2] we use the plane wave basis

$$\phi_{s,p} = \frac{e^{id\kappa s}}{\sqrt{L}}b_p(\kappa),$$

where L eventually tends to infinity. In so doing, the quasimomentum κ belongs to the interval $[0, \frac{2\pi}{a}\sqrt{N})$. We finally arrive at the following equation, where we have put $\theta = 2\pi\alpha N^{-1}$:

$$\begin{aligned}&-\frac{J_x}{2}(e^{-i\theta qp+iqd\kappa}b_{p+r} + e^{i\theta q(p-r)-iqd\kappa}b_{p-r})\\ &-\frac{J_y}{2}(e^{i\theta rp-ird\kappa}b_{p+q} + e^{-i\theta r(p-q)+ird\kappa}b_{p-q}) + edFpb_p\\ &= Eb_p.\end{aligned} \tag{21}$$

Equation (10) in Sec. II A is the particular case $(r,q) = (0,1)$ of this more general equation. It is also possible to show (see Appendix) that in the semiclassical approach this equation yields the classical Hamiltonian (14), after applying a canonical transformation.

B. Rotated basis

In this method we do not introduce sublattices but diagonalize the Hamiltonian by changing the basis. One begins with the tight-binding Hamiltonian in the gauge (17) as before, that is, Eq. (18). One then imposes periodicity on the lattice space in the following way: Let K be an even integer, and let us identify lattice points (l,m) and (l',m') if and only if $l - l'$ is an integer multiple of Kq and $m - m'$ is an integer multiple of Kr. The Hamiltonian (18) typically does *not* satisfy this periodicity. Nonetheless observe that by letting K tend to infinity the period can be made arbitrarily large, following the standard approach. At finite K the lattice is then composed of K^2qr distinct points.

Next, we define new lattice period

$$\tilde{d} = a\sqrt{N}$$

and an adimensional quasimomentum $k = \tilde{d}\tilde{\kappa}$, that can take the discrete values

$$k = 2\pi\frac{j}{K}, \quad j = 0,\ldots,K-1, \tag{22}$$

and a new set of basis functions associated with k:

$$\left|\phi^{(\mu)}_{p,k}\right\rangle = \sum_{n=-K/2+1}^{K/2} \frac{e^{ikn}}{\sqrt{K}} |p+qn, \mu - rn\rangle. \tag{23}$$

This definition is consistent with the imposed periodicity on the lattice, as can be seen by letting $n \to n + K$ and observing that the right-hand side does not change. Also observe that if $k \neq k'$

$$\left\langle\phi^{(\mu')}_{p',k'}\middle|\phi^{(\mu)}_{p,k}\right\rangle = 0,$$

for all choices of p,p',μ,μ'. Moreover, keeping k fixed, different functions $|\phi^{(\mu)}_{p,k}\rangle$ and $|\phi^{(\mu')}_{p',k}\rangle$ overlap if and only if (p,μ) and (p',μ') belong to the same discrete transverse line of direction $(q,-r)$; i.e., there exists an integer j such that $(p',\mu') = (p,\mu) + j(q,-r)$. In this case,

$$\left\langle\phi^{(\mu-jr)}_{p+jq,k}\middle|\phi^{(\mu)}_{p,k}\right\rangle = e^{ikj}.$$

The fact that different functions may overlap is clearly a consequence of the overdetermination of the set $|\phi^{(\mu)}_{p,k}\rangle$, which is made of K^3rq elements: The integer variables p and μ can take all values from 0 to $Kq-1$, and from 0 to $Kr-1$, respectively, while k can take the K discrete values in Eq. (22). To the contrary, as observed above, the periodic lattice requires a basis of K^2rq elements only. Since for each pair (p,μ), the function $|\phi^{(\mu)}_{p,k}\rangle$ is a linear combination of K lattice sites $|l,m\rangle$, it is easy to see that this set can be equally spanned by keeping (p,μ) fixed and letting k vary over the K discrete values in Eq. (22). It is equally easy to find that the full periodic lattice can then be spanned by choosing (p,μ,k) in the discrete set $\mathcal{I}$:

$$\mathcal{I} = \{0,\ldots,Kq-1\} \times \{0,\ldots,r-1\} \times \left\{0, 2\pi\frac{1}{K},\ldots,2\pi\frac{K-1}{K}\right\}.$$

We remark that in the set $\mathcal{I}$ the variable μ takes on a restricted set of values, of cardinality r. Equivalently, we could have chosen a set organized in strips parallel to the m axis, but since $r \leqslant q$, this choice would have been less convenient. To sum up, we have introduced the basis for the periodic lattice that, because of the above computations, is composed of orthonormal functions.

Let us now compute the matrix elements of $\widehat{H}$ over this basis. The fundamental point is that $\widehat{H}$ does not couple functions with different k. In fact, when computing the nondiagonal couplings, the product $rl + qm$ appears, which is constant on the transverse lines defined above. The sum over n of the phases stemming from Eq. (23) is then zero, unless $k = k'$. The same result also holds for the diagonal term $(F_x l + F_y m)$, since (F_x,F_y) is proportional to (r,q); see Eq. (16). Observe that this is true at any finite value of K, independently of the fact that the Hamiltonian $\widehat{H}$ is, or is not, periodic. Therefore, the spectral problem of $\widehat{H}$ over the periodic lattice decomposes into the K fibers obtained by letting $k = 2\pi\frac{j}{K}$, with j fixed. At this point one is left with the computation of the matrix elements within a fiber.

Suppose now that $1 < r < q$; we shall treat the remaining cases $1 = r \leqslant q$ separately. Then, by explicit calculation we find that the nonzero matrix elements of $\widehat{H}$ are the following. The "horizontal" coupling leads to the matrix element

$$\left\langle\phi^{(\mu)}_{p+1,k}\middle|H^h\phi^{(\mu)}_{p,k}\right\rangle = -\frac{J_x}{2}\exp\left(i2\pi\alpha\frac{q}{N}(rp+q\mu)\right),$$

if $0 \leqslant p \leqslant Kq-2$, while for $p = Kq-1$

$$\left\langle\phi^{(\mu)}_{0,k}\middle|H^h\phi^{(\mu)}_{Kq-1,k}\right\rangle = -\frac{J_x}{2}\exp\left(i2\pi\alpha\frac{q}{N}[r(Kq-1)+q\mu]\right).$$

The "vertical" coupling gives

$$\left\langle\phi^{(\mu+1)}_{p,k}\middle|H^v\phi^{(\mu)}_{p,k}\right\rangle = -\frac{J_y}{2}\exp\left(-i2\pi\alpha\frac{r}{N}(rp+q\mu)\right),$$

if $0 \leqslant \mu \leqslant r-2$, while for $\mu = r-1$

$$\left\langle\phi^{(0)}_{p+q,k}\middle|H^v\phi^{(r-1)}_{p,k}\right\rangle = -\frac{J_y}{2}\exp\left(-i2\pi\alpha\frac{r}{N}[rp+q(r-1)]\right)e^{ik},$$

where $p+q$ on the left-hand side is to be understood modulus Kq. The above are half of the required formulas; we must also add the Hermitian conjugate matrix elements. Finally, the diagonal coupling is

$$\left\langle\phi^{(\mu)}_{p,k}\middle|H^d\phi^{(\mu)}_{p,k}\right\rangle = \frac{eaF}{\sqrt{N}}(rp+q\mu).$$

Observe finally that this lattice problem can be seen as a combination of r coupled, one-dimensional, periodic lattice problems of size Kq. This takes a particularly simple form in the case $(r,q) = (1,q)$. In fact, we end up with the single, one-dimensional lattice of size Kq, on which the fiber Hamiltonian

has matrix elements

$$\langle \phi^{(0)}_{p',k} | H \phi^{(0)}_{p,k} \rangle = -\frac{J_x}{2}(e^{i\theta qp}\delta_{p',p+1} + \text{H.c.}) - \frac{J_y}{2}(e^{-i\theta qp}e^{ik}\delta_{p',p+q} + \text{H.c.}) + \frac{eaFp}{\sqrt{N}}\delta_{p',p}. \tag{24}$$

We are therefore equipped with the analytical tools to compute the energy spectrum of the system.

The right panel in Fig. 1 displays an example of the spectrum for $(r,q) = (1,1)$, which was calculated by either of two methods. Note that spectrum is periodic on the quasimomentum with the period $2\pi/\tilde{d} = (2\pi/a)/\sqrt{N}$. Also note that both spectra in Fig. 1 show the characteristic pattern with straight lines; moreover, the slope of the lines is the same in both panels. As will be shown later on, this slope defines the velocity of quantum particle in the transporting regime.

C. Continuity properties of the spectrum

In the preceding paper [1], both theoretically and in the numerical examples, we have considered rational and small values of α, a fact that assured both periodicity of the reduced one-dimensional Hamiltonian in (10) and validity of the semiclassical analysis. In this section we discuss the spectral properties of the Hamiltonian (1) for the case of a general value of α, but still rational values of the field direction β.

As remarked in the introduction, it is instructive to think of the limiting case of null magnetic and electric field: The spectrum is absolutely continuous, composed of a single band. Keeping the electric field null, while turning on the magnetic field, the one-dimensional Hamiltonian (10) [or equally well the Hamiltonian (21)—being the electric field null, the two are equivalent], becomes the celebrated Harper Hamiltonian, whose spectrum has bands for rational values of α [12]. Therefore, the spectrum of the original two-dimensional Hamiltonians (9) and (18) is also absolutely continuous. For irrational values of α, the spectrum of (10), (21) is absolutely continuous (for $J_y > J_x$), pure point (for $J_y < J_x$), or singular continuous, in the critical case $J_x = J_y$. In the first case, obviously, the spectrum of (9), (18) is absolutely continuous. Interestingly, the same is true also in the second case, $J_y < J_x$: By varying the quasimomentum associated with the invariant direction x, the eigenvalues of (10) and (21), which exist since the spectrum is point, *move and draw* the energy bands of (9) and (18). Finally, for $J_x = J_y$, since in this case the spectrum of (10), (21) is the same for almost all values of κ, due to ergodicity of the Hamiltonian, the spectrum of (9), (18) is also singular continuous. This is the complete description in the case of null electric field.

The previous results are classical in historical sense. They are useful to understand the nonzero electric field case. Since β is rational, we can still use the Hamiltonians (18), (21). In this case the spectrum of the one-dimensional Hamiltonian (21) is pure point for any value of α—whether rational or irrational, small or large. Therefore, we typically expect the spectrum of (18) to be absolutely continuous, drawn by the eigenvalues $E_\nu(\kappa)$. Of course, this is heuristic discussion is not a substitute for a rigorous proof, but it can give us a hint into the physical phenomenon. We therefore conjecture that for any value of α, and nonzero electric field with a rational direction ratio, the spectrum is absolutely continuous. Quantum dynamics under these circumstances should reflect the spectral properties and be ballistic. We shall prove numerically that this is indeed the case.

D. Strong-field limit and perturbation theory

In the strong-field limit we can find analytic approximations of the spectrum by perturbation theory based on Eq. (21). These results are independent of the rationality of α and of its amplitude. The case $\beta = 0$ has been described in Sec. II D. The next simplest case is $\beta = 1$; i.e., $(r,q) = (1,1)$. In this case, it is convenient to rewrite Eq. (21) in the form

$$-[V(p;\kappa)b_{p+1} + V^*(p-1;\kappa)b_{p-1}] + edFpb_p = E(\kappa)b_p,$$

where $V(p;\kappa) = (J_x e^{-i\pi\alpha p}e^{id\kappa} + J_y e^{i\pi\alpha p}e^{-id\kappa})/2$. Similar to the case $(r,q) = (0,1)$ analyzed in Sec. II D, the unperturbed spectrum of the system consists of flat bands separated by the Stark energy; i.e., $E^0_\nu(\kappa) = edF\nu$. However, unlike the case $(r,q) = (0,1)$ the first-order correction to this spectrum vanishes. The second-order correction is given by

$$\Delta E_\nu = \frac{|V(\nu-1;\kappa)|^2}{edF} - \frac{|V(\nu;\kappa)|^2}{edF} = \frac{J_xJ_y}{2edF}\{\cos[2\pi\alpha(\nu-1) - 2d\kappa] - \cos(2\pi\alpha\nu - 2d\kappa)\}.$$

This equation proves that the bandwidths decrease as $1/F$ when F increases. This is a special case of a general perturbation theory result. To treat all other cases (r,q), notice that according to Eq. (21), the Hamiltonian operator can be written as $H = H_0 + V$, with

$$H_0 = \sum_p edFp\ |p\rangle\langle p|, \tag{25}$$

$$V = \sum_p \Phi(p,q,\kappa)|p\rangle\langle p+r| + \Phi^*(p-r,q,\kappa)|p\rangle\langle p-r| + \Theta(p,r,\kappa)|p\rangle\langle p+q| + \Theta^*(p-q,r,\kappa)|p\rangle\langle p-q|, \tag{26}$$

where we have put

$$\Phi(p,q,\kappa) = -\frac{J_x}{2}\ e^{-i\theta qp}e^{iqd\kappa}, \qquad \Theta(p,r,\kappa) = -\frac{J_y}{2}\ e^{i\theta rp}e^{-ird\kappa}. \tag{27}$$

Two properties of this Hamiltonian are immediately noticed. First, as noted above, the unperturbed spectrum is equally spaced. Second, the perturbation V only couples unperturbed states (here, Kronecker deltas at site p) with quantum numbers differing by either q or r. For short, denote by $V_{p,p'}$ the matrix elements of the perturbation V in the unperturbed basis.

When $q > r \geqslant 1$ it is then immediate that the diagonal terms of the perturbation V vanish. Proceed next to consider second-order perturbation theory: It is composed of terms of the kind $|V_{p,p+j}|^2/(E^0_p - E^0_{p+j})$, where E^0_p is the unperturbed spectrum. In our case, j can only take the values $\pm q$, $\pm r$. Yet, for any of these j, the energy difference $(E^0_p - E^0_{p+j}) = -edFj$ is the opposite of that of the term $-j$ (the unperturbed

levels are equidistant), so that the two contributions cancel exactly, and second-order perturbation theory yields a null result.

The last observation has also a bearing on the general, nth term in the Rayleigh-Schrödinger perturbation series for $n \geqslant 3$, which contains the second-order term as a factor, among other terms. Typically, the nth term is composed of sums of products, call them Π, of n matrix elements of the perturbation V. The first term in such summation is always of the kind

$$\prod = \frac{V_{p,j_1} V_{j_1,j_2} \cdots V_{j_{n-1},p}}{\left(E_p^0 - E_{j_1}^0\right)\left(E_p^0 - E_{j_2}^0\right) \cdots \left(E_p^0 - E_{j_{n-1}}^0\right)}. \quad (28)$$

Other terms in the summation giving the nth term contain shorter "chains" of products of matrix elements, of length at most $n-1$, appropriately multiplied among themselves to give order n, of course divided by the related denominators. In some of these, the second-order term appears as a factor.

Notwithstanding this complexity, the particular form of the Hamiltonian problem (25), (27) permits us to derive a simple result. In fact, the numerator in Eq. (28) is null unless the "path" $p \to j_1 \to j_2 \to j_{n-1} \to p$ is composed of "allowed" jumps of size $\pm q, \pm r$. It is easy to realize that, in order for this path to comprise the least number of jumps, it must contain a positive number, s, of steps of length q and a negative number, t, of steps of length r (or the same with opposite signs), so that $sq + tr = 0$. Now, since q and r are relatively prime, the minimal solutions are $s = r, t = -q$ or $s = -r, t = q$. This implies that the minimal number of steps must be $n = r + q$. Therefore, when $q > r \geqslant 1$ the first nonzero term in the Rayleigh-Schrödinger perturbation series for the eigenvalues is of order $n = p + q$ and is composed of $2\binom{q}{p+q}$ addenda of the form (28). All other terms that appear formally in the analytical expression for the nth term contain shorter "chains" (and/or the second-order term) and are therefore null.

The complete expression of the leading perturbation term can be explicitly computed, using Eq. (27). Yet, notice that all terms of the form (28) contain the common factor

$$\Lambda_{r,q}(F) = \frac{(-J_x)^q (-J_y)^r}{2^{q+r} F^{q+r-1}}, \quad (29)$$

and therefore we can write

$$E_\nu(\kappa) \simeq E_\nu^0 + \Lambda_{r,q}(F) P_n(\kappa), \quad (30)$$

where $P_n(\kappa)$ is a trigonometric function of the quasimomentum κ. A consequence of this result is that the rate of ballistic spreading discussed in Sec. II D is strongly suppressed for large electric field as soon as the vector $\mathbf{F}$ does not point to a strongly rational direction β. Later on, in Sec. VI B, we confirm this expectation, as well as the quantitative dynamical estimates that follow from Eqs. (29) and (30).

V. WAVE-PACKET DYNAMICS: NUMERICAL TECHNIQUES

To simulate numerically the quantum evolution of the system we have adopted two different approaches. In the first, we have used the time-dependent gauge $\mathbf{A}(\mathbf{t}) = \mathbf{A}_0 + c(F_x t, F_y t)$, for which the electric field appears as a periodic driving of the system. For the static vector potential $\mathbf{A}_0$, which is responsible for the magnetic field, we used the Landau gauge $\mathbf{A}_0 = B(0,x)$. This leads to the following Schrödinger equation with explicit time dependence

$$i\hbar \dot{\psi}_{l,m} = -\frac{J_x}{2}(e^{-i\omega_x t}\psi_{l+1,m} + \text{H.c.}) - \frac{J_y}{2}(e^{-i(2\pi\alpha l + \omega_y t)}\psi_{l,m+1} + \text{H.c.}),$$

which we have solved employing the standard Runge-Kutta techniques implemented in MATLAB.

In the second approach, implemented in FORTRAN, we have chosen the time-independent gauge $\mathbf{A} = B(-y,0)$, so that the Schrödinger equation reads

$$i\hbar \dot{\psi}_{l,m} = -\frac{J_x}{2}(e^{-i2\pi\alpha m}\psi_{l+1,m} + e^{i2\pi\alpha m}\psi_{l-1,m}) - \frac{J_y}{2}(\psi_{l,m+1} + \psi_{l,m-1}) + ea(F_x l + F_y m)\psi_{l,m}.$$

The right-hand side of the equation is in the form of the action of a time-independent operator on the two-dimensional lattice vector ψ. We have computed the exponential of this operator using the repeated Chebyshev expansion [13], combined with a numerical truncation of the infinite lattice to a strip along the line of equation $F_x l + F_y m = 0$, that corresponds to the direction of spreading of the wave packet. This is effected numerically by introducing *slanted* integer coordinates $l' = l$ and $m' = m + \text{int}(\frac{F_y}{F_x} l)$. Observe that the directions of increase of l' and m' are no longer orthogonal. Yet, this provides a convenient re-labeling of lattice sites to enforce the strip truncation mentioned above. We always checked that the wave-packet projection at the boundaries of large $|l'|$ and $|m'|$ is smaller than a very low threshold, at any time during the evolution.

The initial conditions, obviously common to both approaches, consisted of two-dimensional Gaussian wave packets, centered at the origin of the lattice, of adjustable widths: $\psi_{l,m} \sim \exp(-C_x l^2 - C_y m^2)$. To simulate an incoherent wave packet, all components $\psi_{l,m}$ have been multiplied by statistically independent random phases $e^{i\vartheta_{l,m}}$, and an average of quantum amplitudes over different realizations of the initial packet has been performed.

Finally, to simulate the dynamics of transporting states we have first constructed them by using the appropriate gauge for the magnetic field and then we have applied a unitary transformation to translate them into the fixed Landau gauge. For example, for the transporting states (13), which were constructed using the gauge $\mathbf{A}_0 = B(-y,0)$, the unitary transformation reads $\psi_{l,m}(t=0) = \exp(-i2\pi\alpha l m)\Psi_{l,m}$.

VI. WAVE-PACKET DYNAMICS: THE SEMICLASSICAL REGION

Let us start our analysis of the system dynamics from the semiclassical region $\alpha \ll 1$. It is instructive to have a pictorial look at four significant cases. We select two values of the field intensity, the first weak, $F = 0.2$, and the second strong, $F = 0.5$. We combine these with two values of the orientation of the electric field: a rational value, $\beta = 2/3$, and a strongly irrational one, $\beta = (\sqrt{5}-1)/2$.

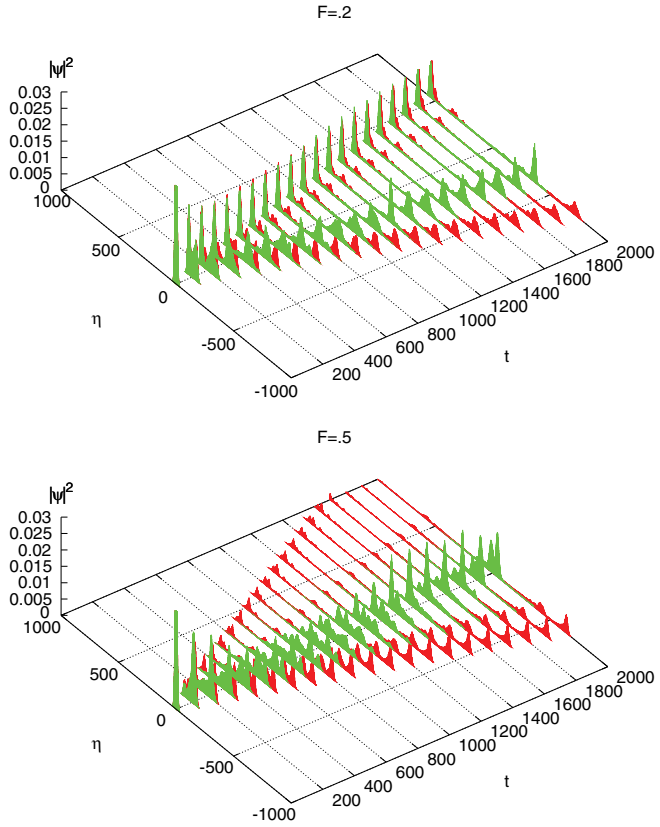

FIG. 5. (Color online) Wave-packet amplitudes $|\psi(\eta,t)|^2$ versus η and time, averaged over 12 realizations of the initial incoherent wave function, for $J_x = J_y = 1$, $\alpha = 1/10$, and two electric field orientations: $\beta = 2/3$ (red curve, darker tone) and $\beta = (\sqrt{5}-1)/2$ (green curve, lighter tone). Electric field amplitude is $F = 0.2$ (top) and $F = 0.5$ (bottom).

Since the wave packet spreads in the direction of the η coordinate of the rotated frame of reference in Eq. (19), we find it convenient to adopt this coordinate system. Moreover, since we observe that the wave packet is localized in the ξ direction, we compute the wave-packet projected amplitude $|\psi(\eta,t)|^2 = \sum_\xi |\psi(\eta,\xi,t)|^2$.

In Fig. 5 we display $|\psi(\eta,t)|^2$ after averaging this quantity over a number of different realizations of the random phases in the initial Gaussian wave packet. In the first case, Fig. 5(a), the electric field amplitude is $F = 0.2$. We observe for both orientation of the field subpackets moving at constant speed, in the positive and negative η directions. The situation changes radically in Fig. 5(b), drawn on the same scale, now for $F = 0.5$. Here, we find subpackets traveling in both directions only in the case of rational orientation of the field, while in the irrational case we observe localization of the motion also in the η direction.

To the contrary, the projected distributions on the ξ direction (not reported here), initialized to a Gaussian, settle to a shape that is still approximately Gaussian, whose width naturally depends on the amplitude of the electric field: a clear sign of Stark localization in the direction of the electric field, which does not depend on the orientation of this latter. Let us now consider separately the weak- and strong-field cases.

A. Weak-field limit and transporting states

Suppose now that conditions (6) hold. Then, according to Sec. III, $F < F_{cr}$ and the system has transporting islands. The quantum-mechanical signature of these islands is straight lines in the energy spectrum, which are clearly observed in Fig. 1. The slopes of these lines coincide with the drift velocity v^* of Eq. (5).

Adapting Eq. (13) of Sec. II B to the present case of rational field direction, we can construct a family of localized wave packets, which move at the drift velocity in the direction orthogonal to the field, without changing their shape. To do this, we first write these states on the extended lattice that, we recall, consists of N sublattices:

$$\Phi_{s,p} = \int g(\kappa) b_p(\kappa) e^{isd\kappa} d\kappa. \tag{31}$$

In the above, $g(\kappa)$ is an envelope function, that we choose of the form $g(\kappa) \sim \exp[-C(d\kappa/2\pi)^2]$. Then we select from this (generally very large) array only the complex amplitudes $\Psi_{l,m}$ which sit on the original lattice. We plot these states in Fig. 3; the upper row of this figure displays the transporting states $\Psi_{l,m}$ for $(r,q) = (0,1)$ and $(r,q) = (1,1)$, where we choose $C = 1$. For this value of C the states are equally localized in both directions, parallel and orthogonal to the vector $\mathbf{F}$. If C is decreased, the states become more extended in the parallel direction and more localized in the orthogonal direction; see the lower row in the figure. In the opposite case, i.e., when C is larger than one, the situation is obviously reversed. In the limit $C \to \infty$, when $g(\kappa)$ becomes a Dirac δ function, the transporting states are extended Bloch-like waves in the direction orthogonal to the field that carry the current v^* [1].

Figure 6 depicts the results of numerical simulations for $F = 0.1$ and two orientations, $\beta = 1/3$ and $\beta = (\sqrt{5}-1)/4$.

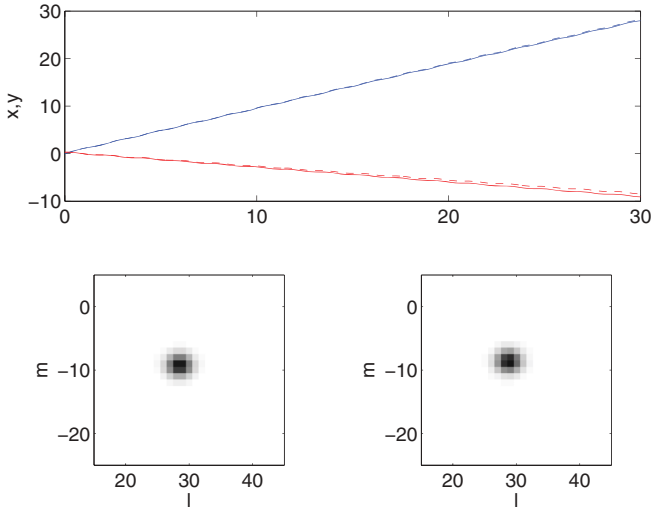

FIG. 6. (Color online) Top panel: The center of gravity of the specially constructed wave packet $x(t)$ (blue, increasing data) and $y(t)$ (red, decreasing data) for $eaF/J = 0.1$ and $\beta = 1/3$ (solid lines) and $\beta = (\sqrt{5}-1)/4$ (dashed lines) versus time, measured in adimensional units t/T_J, where $T_J = 2\pi J/\hbar = 2\pi$ is the tunneling period. The lower panels show the wave packets at the end of numerical simulations, $t/T_J = 30$, depicted as grey tone images (black maximum, linear intensity scale), for these two cases.

Observe that these values are half of those considered in the previous subsection. As initial condition we choose the wave packet shown in the upper-left panel of Fig. 3. This packet is the transporting state for the field direction $(r,q) = (0,1)$. In this family, it is the easiest to construct numerically. Moreover, when F is small, it has large overlap with transporting states for nearby directions as well and it can be used to test the transporting regime for arbitrary field directions. The solid lines in panel (a) of Fig. 6 show the wave-packet center of gravity $(x(t), y(t))$ for $\beta = 1/3$. It is seen that the packet moves in the direction orthogonal to the electric field, $y(t) = -\beta x(t)$, and that the speeds in the two directions are those predicted by semiclassical analysis. The dashed lines show the same quantities, now for $\beta = (\sqrt{5}-1)/4$. The lower panel shows the wave packets at the final time of numerical simulations, which appears to be still well focused. This confirms the fact that in this short-time, semiclassical regime, dynamics is not affected by commensurability of Bloch frequencies. We comment later on the long-time regime.

When the initial wave function is not in the form of a transporting state, we encounter different dynamical behaviors. If the initial packet overlaps significantly a transporting state, we observe a comet-like dynamics with the comet head moving at the drift velocity and the tail extending in the opposite direction. Finally, for a generic initial state with small overlap with the transporting state, the wave-packet dynamics is an asymmetric ballistic spreading whose dispersion increases in time approximately as

$$\sigma(t) \approx v^* t/\sqrt{2}.$$

However, the most prominent feature of the weak-field, semiclassical regime (6) is that it is insensitive to the rational versus irrational nature of the orientation β, i.e., to the commensurability of the Bloch frequencies. This conclusion is consistent with the semiclassical analysis.

B. Strong-field limit

In the large-field limit, $eaF/2\pi J > \alpha$, the scaling law (29), (30) implies that dispersion of a wave packet is inhibited for irrational field directions. Therefore, the quantum motion can only oscillate in width and position. On a relatively short time scale, this is also the case for "bad" rationals r/q with $r,q \gg 1$, while ballistic spreading can be detected only for $\beta = r/q$ with a small denominator.

In the original frame of reference (x,y) the motion can be well described by the first momenta $x(t)$ and $y(t)$ and by the dispersion $\sigma^2(t) = a^2 \sum_{l,m}(l^2+m^2)|\psi_{l,m}(t)|^2 - x^2(t) - y^2(t)$. In Fig. 7 we display these data for an initial Gaussian wave packet with $F = 2$, $\alpha = 1/10$ and for rational $\beta = 1/3$ and irrational direction $\beta = (\sqrt{5}-1)/4 \approx 0.309$. The dashed and solid lines in the lower panel depict the wave-packet dispersion for these two cases, respectively. As expected, a secular increase of the dispersion is observed only in the rational case $\beta = 1/3$. In the upper panel, dashed and solid lines plot $x(t)$ and $y(t)$ in the case of the irrational field direction $\beta = (\sqrt{5}-1)/4$. The characteristic amplitudes and frequencies of oscillations of these quantities are defined by

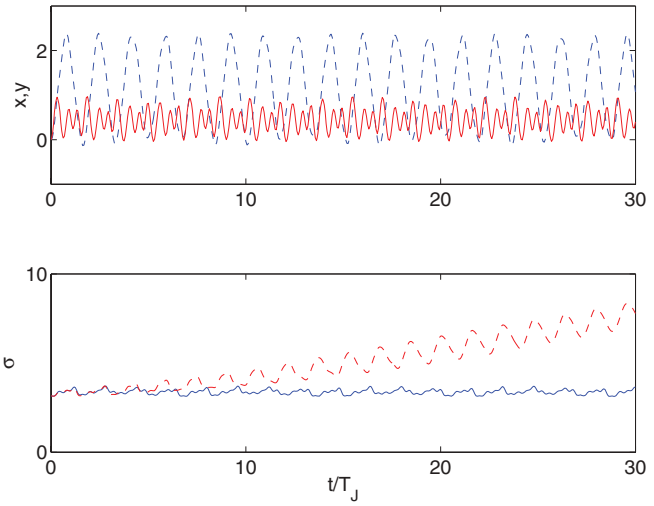

FIG. 7. (Color online) Dynamics of a localized wave packet for $eaF/J = 2$, $\alpha = 1/10$. The upper panel depicts $x(t)$ (dashed blue line) and $y(t)$ (solid red line) for $\beta = (\sqrt{5}-1)/4$. Time is measured in adimensional units t/T_J, where $T_J = 2\pi J/\hbar = 2\pi$ is the tunneling period period. The lower panel shows the wave-packet dispersion in the cases $\beta = 1/3$ (dashed red line) and $\beta = (\sqrt{5}-1)/4$ (solid blue line).

Bloch oscillations,

$$x(t) = \frac{J_x}{2eaF_x}\sin(\omega_x t), \quad y(t) = \frac{J_y}{2eaF_y}\sin(\omega_y t).$$

The magnetic field distorts these oscillations, the more the larger the value of α. In particular, for α close to its maximal value $1/2$ (without any loss of generality one may consider $|\alpha| \leqslant 1/2$) it becomes impossible to recognize Bloch oscillations in the time evolution of the first momenta. Nevertheless, the conclusion that a strong electric field localizes the quantum particle on a lattice remains valid.

When delocalization takes place, it is convenient to consider the rotated coordinate frame (η,ξ). This permits us to verify numerically the scaling law (29), (30). In fact, we expect the coefficient A in the asymptotic growth of the second moment in the η direction,

$$M_2(t) := a^2 \sum_{\eta} |\psi(\eta,\xi)|^2 \eta^2 \sim A^2 t^2,$$

to be proportional to bandwidth and hence, via Eq. (29), to F^{1-q-r}. In Fig. 8 we plot A versus the electric field amplitude F, for five cases of the ratio β, that takes the rational values zero, one, one-half, one-third, and two-thirds. Naturally, the second moment in the field direction ξ is bounded in time. All data sets were computed as averages over different realizations of incoherent Gaussian wave packets with the same initial widths. Values of A were obtained as fits over an asymptotic time range, extending to a few hundreds (in the units adopted) for $\beta = 0$, and to tens of thousands, for $\beta = 2/3$.

Bandwidth affects the dynamics in a second way that might even be more relevant than the first in laboratory experiments. In fact, the indeterminacy principle implies that the time required for the dynamics to "feel" the continuous nature of the spectrum is inversely proportional to bandwidth. We confirmed numerically that the larger the value of $r+q$, the later in time

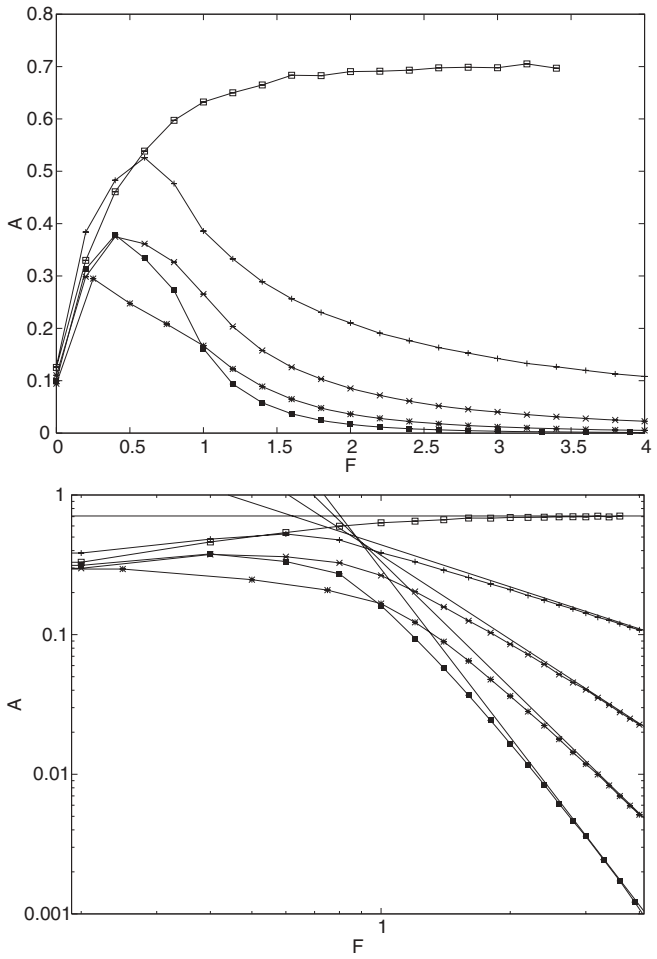

FIG. 8. Top: Coefficient of the asymptotic growth of the second moment in the η direction versus field amplitude F, for $(r,q) = (0,1)$ (open squares); $(r,q) = (1,1)$ (pluses); $(r,q) = (1,2)$ (crosses); $(r,q) = (1,3)$ (asterisks); and $(r,q) = (2,3)$ (full squares). Here, $\alpha = 1/10$. Symbols are joined by lines to guide the eye. Bottom: The same, now displayed in doubly logarithmic scale. The straight lines are the large-field estimates $A \sim F^{1-q-r}$.

the asymptotic behavior is achieved: The packet needs more time to unfold and to "pick up speed." At fixed, large F, the packet seems to be "frozen" for times that grow exponentially in $q + r - 1$, Eq. (8).

VII. QUANTUM DYNAMICS IN THE GENERAL CASE

In the preceding section we have considered small values of α, which insures the semiclassical analysis, which obviously describes the quantum motion appropriately only over a finite time scale. In this section we discuss the extension to the general case.

A. Rational orientation, general Peierls phase

We have already commented that, for rational orientations β, the spectrum should be absolutely continuous for any value of the Peierls phase α. Quantum dynamics under these circumstances should reflect the spectral properties and be ballistic even outside the semiclassical region [15].

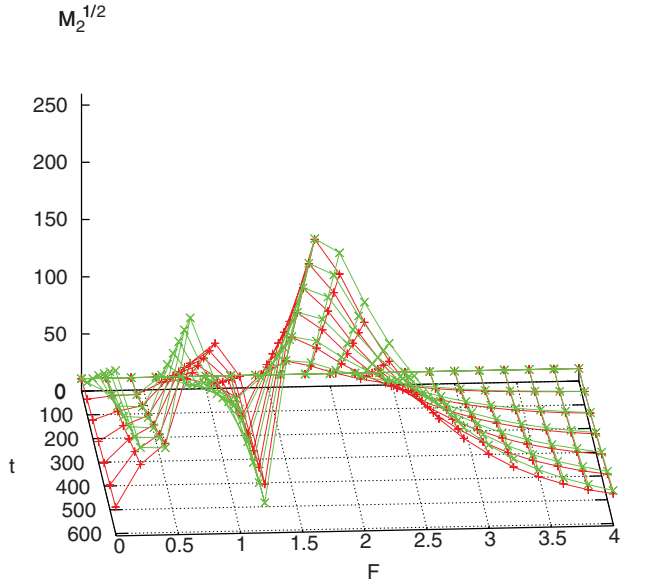

FIG. 9. (Color online) Square root of the second moment $M_2^{1/2}$ in the evolution of an incoherent wave packet versus time t and field intensity F, for $\alpha = 1/3$ (green lines, lighter tone, crosses) and $\alpha = (\sqrt{5}-1)/4$ (red lines, darker tone, pluses). The field is directed as $(1,1)$.

This expectation is confirmed by numerical experiments. In Fig. 9 the square root of second moment is shown versus time and field intensity F for two (large) values of the Peierls phase, $\alpha = 1/3$ and $\alpha = (\sqrt{5}-1)/4 \sim 0.3090$. The orientation is rational: $\beta = 1$. As usual, the incoherent packet is obtained averaging over realization of random phases. We observe two regions in the plot: As expected, for large F data are described by perturbation theory, and no difference between the rational and irrational case is observed. To the contrary, for small F two maxima in the ballistic speed (i.e., the slope of the linear growth of $\sqrt{M_2}$) are observed, with a significant depth between them at around $F = 1.25$. Clearly, this feature is outside the reach of semiclassical analysis. Moreover, the smaller the value of F, the larger become the differences between the rational and irrational case. At null field, of course, exact analysis predicts ballistic motion for rational α and anomalous diffusion, i.e., quantum intermittency [16,17] for irrational α.

To sum up, for rational β we find novel behaviors outside the semiclassical region only in the case of small electric fields. Yet, these novel behaviors are at most variations inside a general picture of ballistic regime.

B. Irrational orientation, general Peierls phase

Finally, we consider the case of irrational directions of the electric field. Here, the Hamiltonians (20) and (21) are not applicable, or rather they can be used in a sequence of rational approximations (r,q) to an irrational direction. It seems therefore that in the perturbative regime the bandwidth (which drives the speed of ballistic spreading, as well as the time required to start this dynamical regime) is smaller than any negative power in the field intensity F. Yet, it could be a nonanalytic function of this latter. This implies that the wave

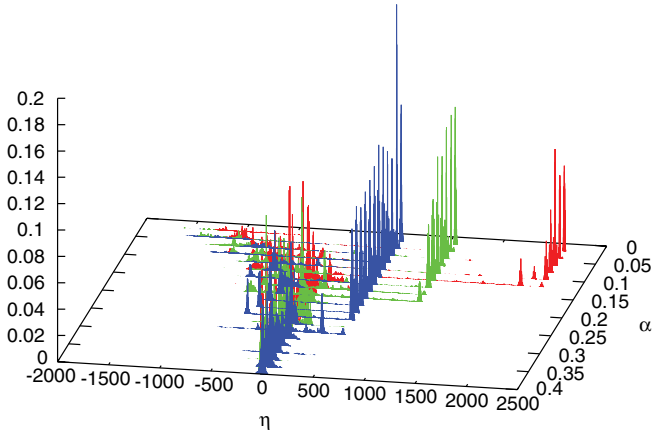

FIG. 10. (Color online) Final wave-packet amplitudes at time $t = 5000$, versus η and α, with $v^* = 0.5$ (red, rightmost packet), $v^* = 0.25$ (green, second from the right), and $v^* = 0.125$ (blue, third packet from the right). In this plot, $\beta = (\sqrt{5}-1)/2$. In addition to the "classical" subpackets traveling in the positive η direction we observe stationary populations on the sites near the origin and quantum tails in the negative η direction.

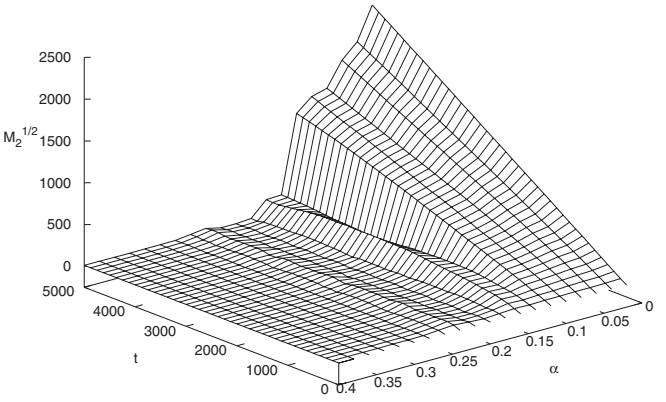

FIG. 11. Dispersion $M_2^{1/2}$ of the wave packet versus time t and α, for $v^* = 0.5$.

packet is localized for large electric field at any irrational direction β.

For small α semiclassical analysis (insensitive to the rationality of the direction) indicates that the motion should be ballistic when $F < F_{\rm cr}$, i.e., $F < 2\pi\alpha J/ea$, a fact confirmed by numerical experiments (see Fig. 5). We expect this behavior to hold until deviations from the semiclassical theory emerge. In fact, the problem of the spectral type for any electric field intensity should be treated along the lines of [9]: This analysis should yield the result that the spectrum is pure point, and quantum motion is localized, albeit the localization length may be very large, as typically happens in two-dimensional systems [14].

Recall that the classical Hamiltonian (14) depends only on the scaled electric field $\mathcal{F}$ and its orientation β. Keeping the direction β fixed, as well as $J = J_x = J_y$, yields a single free classical parameter $F/2\pi\alpha J$, where F is the amplitude of the electric field. It turns out that this ratio coincides with the velocity v^* times the dimensional constant $\hbar/Jea^2$ (that in the units employed in this work takes the value one). It is therefore interesting to study the quantum dynamics at fixed v^*, while varying the semiclassical parameter α. As a consequence, during this scan, the electric field amplitude scales as $F = 2\pi\alpha J v^*$. Again, we observe two quite distinct dynamical regions. First, for values of the classical parameter v^* larger than one, the motion is always localized about the origin, for any nonzero value of α.

To the contrary, a rich dynamical behavior is observed for values of v^* smaller than one. In Fig. 10 we draw the η projection of the evolved wave-packet amplitude versus α, for three values of the classical parameter v^*, and for the irrational value $\beta = (\sqrt{5}-1)/2$. A coherent subpacket moving in the positive η direction is observed in all cases, roughly independent of the value of α, for small values of this parameter. Clearly, this feature should be ascribed to the classical dynamics. The region of α in which this subpacket is observed diminishes when increasing v^*, and disappearance of the packet is abrupt. For values of α larger than this critical threshold, the packet remains localized about the origin.

In Fig. 11 we plot the dispersion of the evolving wave packet as a function of time and α, for $v^* = 0.5$. The changing dynamical behavior for increasing α noted in the previous figures is observed also here: One sees an initial ballistic motion followed by a slower diffusion and by saturation. These numerical data provide us rough estimates of the transition time and the localization length. Notice that in this figure α is proportional to the field intensity F. One could therefore expect a sharp dependence of localization length on the external electric field, in line with the theoretical remarks presented at the beginning of this section.

VIII. CONCLUSIONS

In our previous work [1] we considered the wave-packet dynamics of a quantum particle in a square 2D lattice in the presence of a magnetic field normal to the lattice plane and an electric field, which was aligned along one of the prime axes of the lattice (for definiteness, the y axis). In this work we have extended these studies to the case of arbitrary direction of the electric field vector $\mathbf{F}$. We have confirmed a conjecture put forward in Ref. [1]: Depending on the electric field magnitude, the system has two qualitatively different dynamical regimes, which we refer to as the strong- and weak-field regimes, respectively.

The new analysis has extended the validity of the theory developed in [1] and established new phenomena. For instance, we have used semiclassical analysis to predict ballistic delocalization for small electric field intensities, and arbitrary field directions. Under these conditions, we have used spectral theory to construct nonspreading wave packets traveling at constant speed, at least for finite times.

In fact, for weak electric field the wave-packet dynamics is governed by the cyclotron dynamics. This means that the packet moves in the direction orthogonal to $\mathbf{F}$ at the drift velocity v^*, which is proportional to F, in close analogy with the problem of a charged particle in a free space subjected to crossing electric and magnetic fields. However, the presence of the lattice restricts this behavior to a subspace of initial conditions discussed in Sec. VI A. For generic initial conditions we have found that the packet typically splits

into several packets moving in the orthogonal direction with different velocities, both positive and negative.

In the strong-field regime the wave-packet dynamics is governed by the Bloch dynamics of a quantum particle in a 2D lattice. For null magnetic field, in these Bloch oscillations the packet oscillates near its initial position. The obvious exception to this oscillatory behavior occurs when the vector **F** points to the y direction. Here the packet spreads ballistically in the direction orthogonal to the field at a rate defined by the hopping matrix element. A finite magnetic field "generalizes" this exception to the cases where the vector **F** points to a rational direction, i.e., $\beta = r/q$, with r,q being co-prime numbers. However, now the rate of ballistic spreading in the direction orthogonal to the field is suppressed by a numerical factor proportional to $(1/F)^{(r+q-1)}$. This functional dependence implies that in practice the wave-packet spreading can be detected only for simple rational directions with a small denominator q.

We have found a critical field magnitude $F_{\rm cr}$, which separates in the parameter space the above discussed regimes, by generalizing the semiclassical approach of Ref. [1]. This results in a strongly nonlinear 1D classical system with quasiperiodic driving. Surprisingly, this effective system appears to be completely integrable in spite of the quasiperiodic character of driving, which is a rather rare instance from the view point of dynamical system theory.

Finally we discussed the validity of the semiclassical approach. For irrational directions β, at fixed time and classical parameter $\mathcal{F}$, we observe a sharp suppression of ballistic spreading, occurring when α overcomes a certain threshold. Combined with results for rational directions β, this fact leads us to the conclusion that the energy spectrum of the system is continuous for rational β and pure point for irrational β. This result holds for any value of the Peierls phase α, both rational and irrational.

ACKNOWLEDGMENTS

We thank Jean Bellissard and Italo Guarneri for illuminating comments on the nature of the energy spectrum for irrational β. Computations for this work have been performed on the CSN4 cluster of INFN in Pisa. G.M. acknowledges the support of MIUR-PRIN project "Nonlinearity and Disorder in Classical and Quantum Transport Processes."

APPENDIX: SEMICLASSICAL HAMILTONIANS

Let us obtain Eq. (14) in Sec. III as a semiclassical approximation of Eq. (21). We follow the same lines as in the derivation of Eq. (11) in Sec. II B. As above, when $|\alpha|$ is much less than one, we replace p by the continuous variable ξ and we introduce the shift operator $\exp(\partial_\xi)$. On the left-hand side of Eq. (21) one therefore observes the action of the operator $\mathcal{I}$:

$$\mathcal{I} = -\frac{J_x}{2}\left(\exp\left[-\frac{iar}{\sqrt{N}}i\partial_\xi - 2\pi i\alpha\frac{q}{a\sqrt{N}}\xi\right] + \text{H.c.}\right) - \frac{J_y}{2}\left(\exp\left[-\frac{iaq}{\sqrt{N}}i\partial_\xi + 2\pi i\alpha\frac{r}{a\sqrt{N}}\xi\right] + \text{H.c.}\right) + eF\xi.$$

Next, let us introduce the operators $\tilde{X} = 2\pi\alpha\xi/a$ and $\tilde{P} = -ia\partial_\xi$, which obey the commutation relation $[\tilde{X},\tilde{P}] = 2\pi i\alpha$. The previous equation becomes

$$\mathcal{I} = -J_x\cos\left(-\frac{r}{\sqrt{N}}\tilde{P} + \frac{q}{\sqrt{N}}\tilde{X}\right) - J_y\cos\left(\frac{q}{\sqrt{N}}\tilde{P} + \frac{r}{\sqrt{N}}\tilde{X}\right) + \frac{eaF}{2\pi\alpha}\tilde{X}.$$

Finally, using the canonical transformation $Y = (-r/\sqrt{N})\tilde{P} + (q/\sqrt{N})\tilde{X}$, $P = (q/\sqrt{N})\tilde{P} + (r/\sqrt{N})\tilde{X}$, we obtain the classical Hamiltonian in Eq. (14).

[1] A. R. Kolovsky and G. Mantica, Phys. Rev. E **83**, 041123 (2011).

[2] T. Nakanishi, T. Ohtsuki, and M. Saitoh, J. Phys. Soc. Jpn. **64**, 2092 (1995).

[3] A. Barelli, J. Bellissard, and F. Claro, Phys. Rev. Lett. **83**, 5082 (1999).

[4] H. N. Nazareno and P. E. de Brito, Phys. Rev. B **64**, 045112 (2001).

[5] E. Muñoz, Z. Barticevic, and M. Pacheco, Phys. Rev. B **71**, 165301 (2005).

[6] H. N. Nazareno, P. E. de Brito, and E. S. Rodrigues, Phys. Rev. B **76**, 125405 (2007).

[7] By varying this ratio, interesting dynamical effects can be found: R. Ketzmerick, K. Kruse, D. Springsguth, and T. Geisel, Phys. Rev. Lett. **84**, 2929 (2000). Notice that this paper is limited to the case of null electric field.

[8] J. Bellissard, R. Lima, and E. Scoppola, Commun. Math. Phys. **88**, 465 (1983).

[9] J. Bellissard, in *Trends and Developments in the Eighties*, edited by S. Albeverio and Ph. Blanchard (World Scientific Pub. Co., Singapore, 1985).

[10] J. Bellissard, in *Stochastic Processes in Classical and Quantum Systems (Ascona, 1985)*, Lecture Notes in Physics, Vol. 262 (Springer, Berlin, 1986), p. 2438.

[11] In Ref. [1] we restricted ourselves by considering $g(\kappa) = 1$ if $\pi(2n-1)/a \leqslant \kappa < \pi(2n+1)/a$ and zero otherwise.

[12] A graphic representation of these bands is widely known as Hofstadter's butterfly; see D. R. Hofstadter, Phys. Rev. B **14**, 2239 (1976).

[13] G. Mantica, in *Applications and Computation of Orthogonal Polynomials*, edited by W. Gautschi *et al.*, Internat. Ser. Numer. Math., Vol. 131 (Birkhäuser, Basel, 1999), p. 153.

[14] J. Bellissard (private communication).

[15] We need to remark in this respect that our analysis did *not* confirm in the long-time run the results of Nazareno *et al.* [4], who claimed localization for the case $(r,q) = (1,1)$ and $\alpha = 1/2$.

[16] I. Guarneri and G. Mantica, Phys. Rev. Lett. **73**, 3379 (1994).

[17] G. Mantica, Electron. Trans. Numer. Anal. **25**, 409 (2006).